

Article

Molecular Collective Response and Dynamical Symmetry Properties in Biopotentials of Superior Plants: Experimental Observations and Quantum Field Theory Modeling

Alessandro Chiolerio ^{1,2,*} , Mohammad Mahdi Dehshibi ^{2,3,†} , Giuseppe Vitiello ^{4,*} 
and Andrew Adamatzky ^{2,†} 

¹ Center for Converging Technologies, Bioinspired Soft Robotics, Istituto Italiano di Tecnologia, Via Morego 30, 16163 Genova, Italy

² Unconventional Computing Laboratory, University of the West of England, Bristol BS16 1QY, UK

³ Department of Computer Science and Engineering, Universidad Carlos III de Madrid, Leganés, 28911 Madrid, Spain

⁴ Dipartimento di Fisica “E.R.Caianiello”, Università degli Studi di Salerno, 84013 Fisciano, Italy

* Correspondence: alessandro.chiolerio@iit.it (A.C.); gvitiello@unisa.it (G.V.)

† Current address: The Cyberforest Experiment, Costa Bocche, Paneveggio, 38054 Predazzo, Italy.

Abstract: Trees employ impulses of electrical activity to coordinate actions of their bodies and long-distance communication. There are indications that the vascular system might act as a network of pathways for traveling electrical impulses. A question arises about the correlation and interplay between the molecular (microscopic) level and the macroscopic observable behavior of the system (the electrical impulses), for individual trees and as a component of the larger living ecosystem, the forest. Results from the “Cyberforest Experiment” in the Paneveggio forest (Valle di Fiemme, Trento, Italy) are presented. It is shown that: (i) biopotential features of xylem biomolecular activity can be correlated with the solar (and lunar) cycle, (ii) tree stubs show an electrical molecular activity that is correlated with that of neighboring trees, (iii) statistical features of spike-like peaks and entropy can be correlated with corresponding thermal entropy, and (iv) basic symmetries of the quantum field theory dynamics are responsible for the entanglement phenomenon in the molecular interactions resulting in the molecular collective behavior of the forest. Findings suggest implementing technology that goes in the direction of understanding the language of trees, eventually of fungi, which have created a universal living network perhaps using a common language.

Keywords: molecular electrical biopotential; thermal fluctuations; collective modes; quantum field theory; *Picea abies*



check for updates

Citation: Chiolerio, A.; Dehshibi, M.M.; Vitiello, G.; Adamatzky, A. Molecular Collective Response and Dynamical Symmetry Properties in Biopotentials of Superior Plants: Experimental Observations and Quantum Field Theory Modeling. *Symmetry* **2022**, *14*, 1792. <https://doi.org/10.3390/sym14091792>

Academic Editors: Nicoletta Coccaro and Cosimo Cumbo

Received: 16 July 2022

Accepted: 22 August 2022

Published: 29 August 2022

Publisher’s Note: MDPI stays neutral with regard to jurisdictional claims in published maps and institutional affiliations.



Copyright: © 2022 by the authors. Licensee MDPI, Basel, Switzerland. This article is an open access article distributed under the terms and conditions of the Creative Commons Attribution (CC BY) license (<https://creativecommons.org/licenses/by/4.0/>).

1. Introduction

The increasing demand for tree and forest health monitoring due to ongoing climate change requires new future-oriented and nondestructive measurement techniques [1–5], capable of operating in open air and in rough climate conditions. One such example is given by Electrical Resistivity Tomography (ERT), providing insights into molecular and cellular activity of living trees based on resistivity measurements performed with cross-sectional distribution [6–8]. External factors, such as temperature and water status, have also been evaluated in *Picea abies* individuals [9]. Trees are renowned for their salient intelligence, capability to implement distributed information processing, showing indicators of advanced perception, cognition and adaptive behavior, anticipatory responses, and swarm intelligence [10–14]. Trees employ impulses of electrical activity to coordinate actions of their bodies and long-distance communication [11,15,16]. The bursts of impulses could be either endogenous, e.g., related to motor activities or in a response to external stimulation, e.g., temperature, osmotic environment, rain, wind, mechanical stimulation.

Quite recently, Spontaneous Electrical Low-Frequency Oscillations (SELFOs) have been pointed out as an oscillatory electrical activity of low frequency comprised between 0.01 and 0.1 Hz (the frequency is organism-dependent) that is spontaneously produced and possibly independent of external stimuli and not connected to the external behavior [17]. Electric signals could propagate between any types of cells in a plant tissue; there are indications, however, of higher conductivity of the vascular system which might act as a network of pathways for traveling electrical impulses. Recently, Volkov and Shtessel proved that the electrostimulation of *Aloe vera* induces biopotential fluctuations and communication between the electro-stimulated plants and neighboring plants located in the same or different electrically connected pots regardless if plants are the same or different species [18]. Fungi also exhibit oscillations of their extracellular potential whose complexity has been analyzed in recent studies [19]. We can speculate that when several impulses travel along a vascular network, they meet and interact with other impulses: for example in a tree trunk the vertical impulse movement is triggered by cytoplasm migration, while the horizontal cross-talk is granted by ion diffusion.

The molecular scale is extremely relevant in driving plant physiology; what still remains less explored, is to what extent plant monitoring tools can easily provide feedback about such molecular phenomena. In other words, the question is the one about the correlation and interplay between the molecular (microscopic) level and the macroscopic observable behavior of the system in its biological functional activity, both for individual trees and as a component of the larger living ecosystem, the forest. We are therefore in search of general structural features ruling molecular dynamics so as to provide at the macroscopic level that unitary behavior, the object of our observational tools. In this way, we are led to the study of the symmetry properties characterizing basic molecular dynamics. The nature of such symmetry properties is on one hand related to some common characters of the specific constituent molecules of the system under study, on the other hand, it must carry necessarily some structural aspects able to channel a general dynamical behavior, the same molecular and chemical specificity out of which symmetry emerges. The dynamical symmetries must be able to construct the “wave guide” or the “web” supporting and promoting the observed great functional efficiency of the molecular chemical activity in the biological systems (in the trees in the present case). In this work, we therefore limit ourselves to focus on such general molecular properties, since we are here indeed aiming at describing those symmetry structural aspects able to provide a unified view of local details. The discussion of these latter ones, however, needs to be object of specific analysis.

Thus, since our aim is developing a molecular-based, living information processing system, we monitor the electric potential expressed by plants on a finite number of sites, to observe the entire forest and not a single plant. The electrical response is dependent on the state of the ecosystem that the root structure is embedded into, particularly to the water hydrostatic pressure in the soil. By analyzing the response, one can infer about the root connection graph and the features of environmental and health conditions. Moreover, details about collective behavior of the plants can also be highlighted. To implement a living computing network, we selected a portion of Valle di Fiemme forest located in Paneveggio (TN, Italy) [20–23] including five spots with trees in proximity, of a proper age, spanning approximately 8000 square meters (see Figure 1). Such forest-based information processing devices can be a few hundreds of kilometers in diameter and used to analyze and monitor huge underground ecosystems in an environmentally friendly way. It could be used as a universal molecular query machine to infer morphological features of the root system in real time: e.g., its shape, depth, connectivity patterns, typical root size, distribution in space, hydrostatic pressure, etc., or to query the health of the ecosystem.

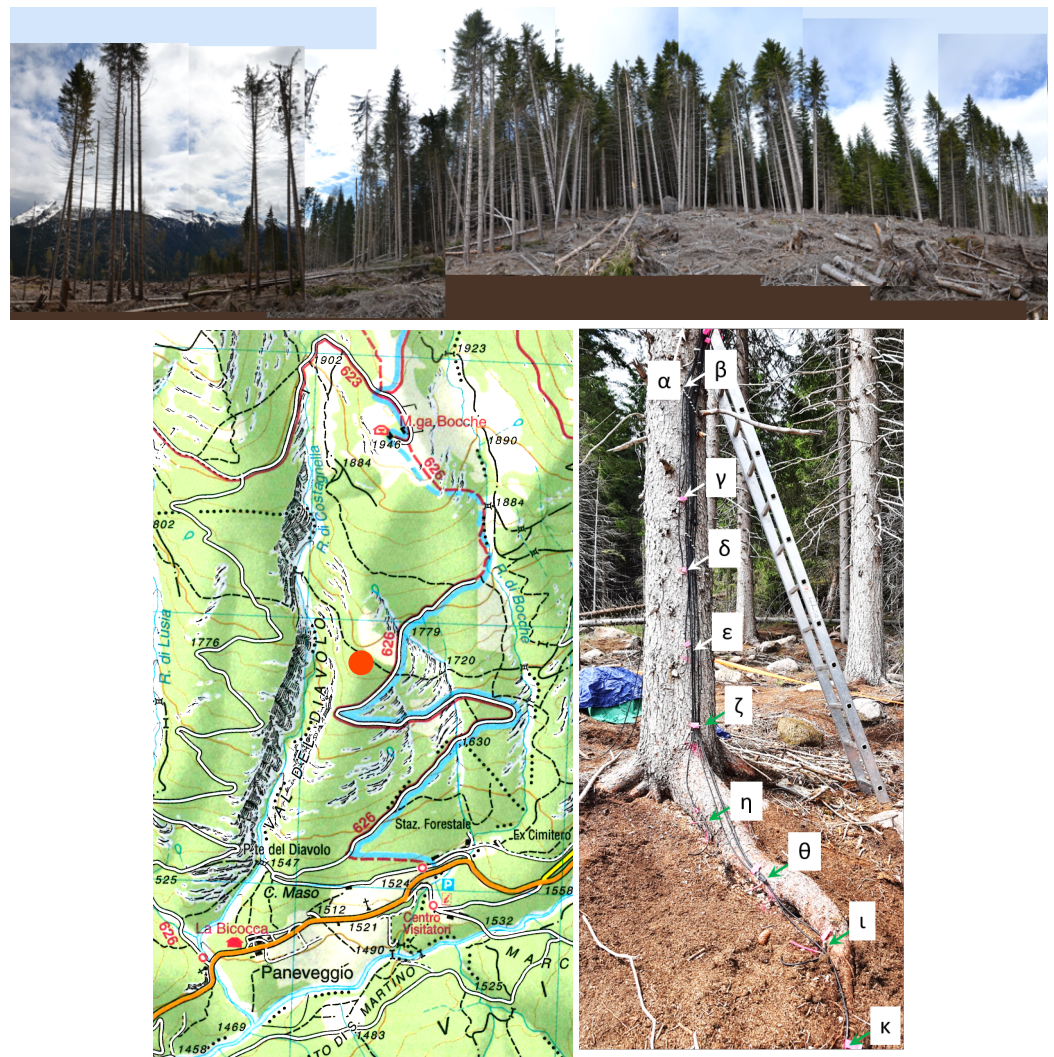


Figure 1. **Top** image: area of the installation in Paneveggio (TN, Italy) seen from a patchwork of camera shots. **Bottom**, from left to right: map showing the exact location of the experiment, indicated by the red circle (diameter corresponding to 100 m); detail showing the geometry of the electrodes inserted in a *Picea abies* tree of approximately 70 years of age, labeled with Greek letters; detail about the box hosting PV modules, battery for powering the infrastructure and WiFi router for collection and data relay, during installation.

The paper is organized as follows. The experimental setup is presented in Section 2. Molecular electrical activity and electrical properties of trees are analyzed in Section 3. A theoretical modeling of the experimental results, pointing to the description of the forest as a collective organism, is sketched on the basis of a quantum field theory framework in Section 3.1. We draw conclusions in Section 4.

2. Materials and Methods

2.1. Experimental

Bio-potentials were collected using stainless steel (AISI 316) threaded rods of 6 mm diameter, positioned along the trunk, uncovered portion of roots and stubs, evenly spaced by 50 cm. The length of the bores was chosen to allow a perfect vertical alignment between the tips of the electrodes. They were isolated, keeping uncovered and electrically conductive the probing tip (1 cm in length) and the back (2 cm in length) where soldering cable lugs were bolted. Each electrode was connected using double shielded ultra low resistance cable INCA1050HPLC from MD Italy for high fidelity audio application, positioned along the trunk using fairleads. A DI-710-US data logger was used in individual channel mode

or differential mode, recording at a frequency of 10 Samples/s per channel, with 16 bit resolution and 100 mV of voltage range. Data were smoothed using a Savitzky-Golay first order function over a variable size window, ranging between 41 and 301 points, depending on the noise floor. Electrodes were labeled with Greek letters: $\alpha, \beta, \gamma, \delta, \epsilon, \eta, \zeta, \theta, \iota, \kappa$. Collection sites were labeled with Latin letters: A, B, C, D, and E. Trees belonging to a collection site were labeled with Arabic numbers: 1, 2, 3, and 4. Resins electronic properties were measured using a Keithley 2635A multimeter for DC characterization (IV curves in the range ± 200 mV and cycles in the range ± 200 V) and an Agilent E4980A precision LCR meter for AC characterization (range from 20 Hz up to 2 MHz, $1 V_{RMS}$) (see also Appendix B.1).

Electrical activity is recorded using several electrodes in mechanical connection with the xilematic tissue, regularly spaced along the trunks, where possible extending down to the roots of the trees, and eventually also to the stubs in the surroundings. Each site hosts 10 electrodes connected to a data logger to collect information in differential mode. Typical measurement chunks cover approximately the duration of a day and highlight the features of superior plant potential oscillations (see Figure 2): the typical bias level varies between 5 and 150 mV, the fluctuation spike-like peak occurs with temporal spacing of 15 ± 50 s (monomodal distribution, median: 4 s, skewness 13, kurtosis 300, maximum interval 1600 s) and has an average amplitude of 10 ± 8 mV (monomodal distribution, mode: 1.5 mV, skewness 2.1, kurtosis 5.8, maximum amplitude 46 mV). Broader structures, lasting tens of minutes, can be associated to the occurrence of sunrise. The diurnal features of biosignal are clearly distinguishable from the nocturnal ones, including a different predominance of low and high frequency noises, as well as a higher number of spikes during night. By tracing sharp peaks, it is possible to observe the propagation delay of stimuli, demonstrating the descending vascular path probed by the electrodes.

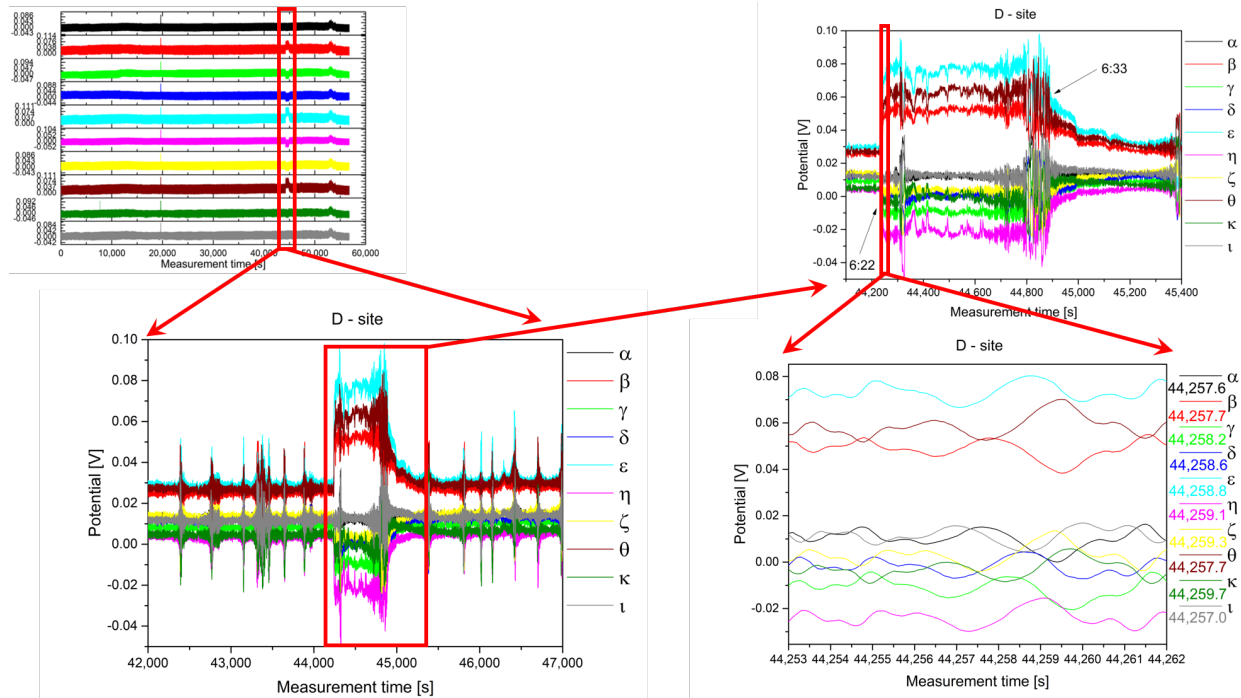


Figure 2. Data measured from site D, tree D1, over ten individual electrodes. Four magnification steps are shown.

2.2. Analysis

We formulated our problem as a Bayesian probability because we are dealing with inferential statistics since we do not have precise information about the underlying distribution of the molecular responses collected from our sensory setup (i.e., unobserved

variable). The cumulative distribution function (CDF) depicts the probability that a random variable X can be found with a value equal to or less than a particular x . The CDF's inverse distribution function, on the other hand, expresses the reciprocal of a random variable and provides the value associated with a certain cumulative probability. We use it to find spike occurrences in the Bayesian context of prior distributions and posterior distributions for scale parameters because we are dealing with modeling phenomena where numerically significant values are more probable than the case for normal distribution.

For the acquired signal x , we use Equation (1) to calculate the inverse of the standard normal CDF.

$$x = F^{-1}(p|\mu, \sigma) = \{x : F(x|\mu, \sigma = p)\}, \quad (1)$$

where μ is the mean, σ is the standard deviation, and $p = F(x|\mu, \sigma) = \frac{1}{\sigma\sqrt{2\pi}} \int_{-\infty}^x e^{-\frac{(t-\mu)^2}{2\sigma^2}} dt$. The standard normal distribution has zero mean and unit standard deviation, and the result x is the solution of the integral equation where we supply the desired probability p .

Assume $\mathcal{X} = \{(t_i, x_i)\}_{i=1}^{\mathbb{C}}$ is a recording set of \mathbb{C} channels with the entire length of T seconds and samplings rate of f_s Hz, where $x = \max(x) - x$ defines the signal's sample value at time t , $1 \leq t \leq T$. Our objective is to detect the set of spike events $\mathcal{S} = \{s_1, s_2, \dots, s_\eta\}$, where $\eta \ll T$. A spike event (i.e., a local peak) is a data sample that is either greater than the two neighboring samples or equal to ∞ . We calculate the following complexity measurements by locating the local peaks.

1. Spike number: Total number of located peaks.
2. Barcode entropy: We represent the entire recording duration T with a binary string \mathcal{S} , with '1 s' indicating the availability of spike events and '0 s' otherwise. The Shannon entropy of this binary string (i.e., barcode entropy) is calculated by $H(\mathcal{S}) = -\sum_i p(s_i) \log p(s_i)$.
3. Simpson index: It is calculated as $Simpson = \sum_{w \in W} (v(w)/\eta)^2$. It linearly correlates with Shannon entropy for $H < 3$ and the relationship becomes logarithmic for higher values of H . The value of *Simpson* ranges between 0 and 1, where 1 represents infinite diversity and 0 no diversity.
4. Space filling (D) is the ratio of non-zero entries in W to the total length of string.
5. Expressiveness (E) is calculated as the Shannon entropy H divided by space-filling ratio D , where it reflects the 'economy of diversity'.
6. Lempel–Ziv complexity (LZ) is used to assess temporal signal diversity, i.e., compressibility. We use the Kolmogorov complexity algorithm [24] to measure the Lempel–Ziv complexity.
7. Rényi (R_q) [25] and Tsallis (Tq) [26] additive entropy concepts are generalizations of the classical Shannon entropy. Regardless of the generalization, these two entropy measurements are used in conjunction with the Principle of maximum entropy, with entropy's main application being in statistical estimation theory. Tsallis and Rényi entropy measurements are expressed as $T_q(p_i) = \frac{k}{q-1} \left(1 - \sum_i p_i^q\right)$ and $R_q(\mathcal{S}) = \frac{1}{1-q} \log\left(\sum_i p_i^q\right)$, where q is the *entropic-index* or Rényi entropy order with $q \geq 0$ and $q \neq 1$, which in our experiments was set to 2.

We underline, however, that Bayesian statistics is appropriate to study the underlying distribution of unobserved molecular responses that generate electrical fluctuations.

3. Results

When measurements are studied in the frequency domain by using Fast Fourier Transform (FFT), the outcomes are that above approximately 200 mHz the Total Impulse Square Amplitude become almost perfectly horizontal and show no clear features, while at lower frequencies' typical features appear showing fingerprints in the 1 to 10 mHz range (see Figure 3). The Short Time Fourier Transform (STFT) is also a powerful tool to visualize the different features of diurnal signals versus nocturnal ones. The different pace, showing

a high frequency nocturnal activity and a more quiet diurnal one, can be justified by a higher degree of inner disorder and will be discussed in Section 3.1.

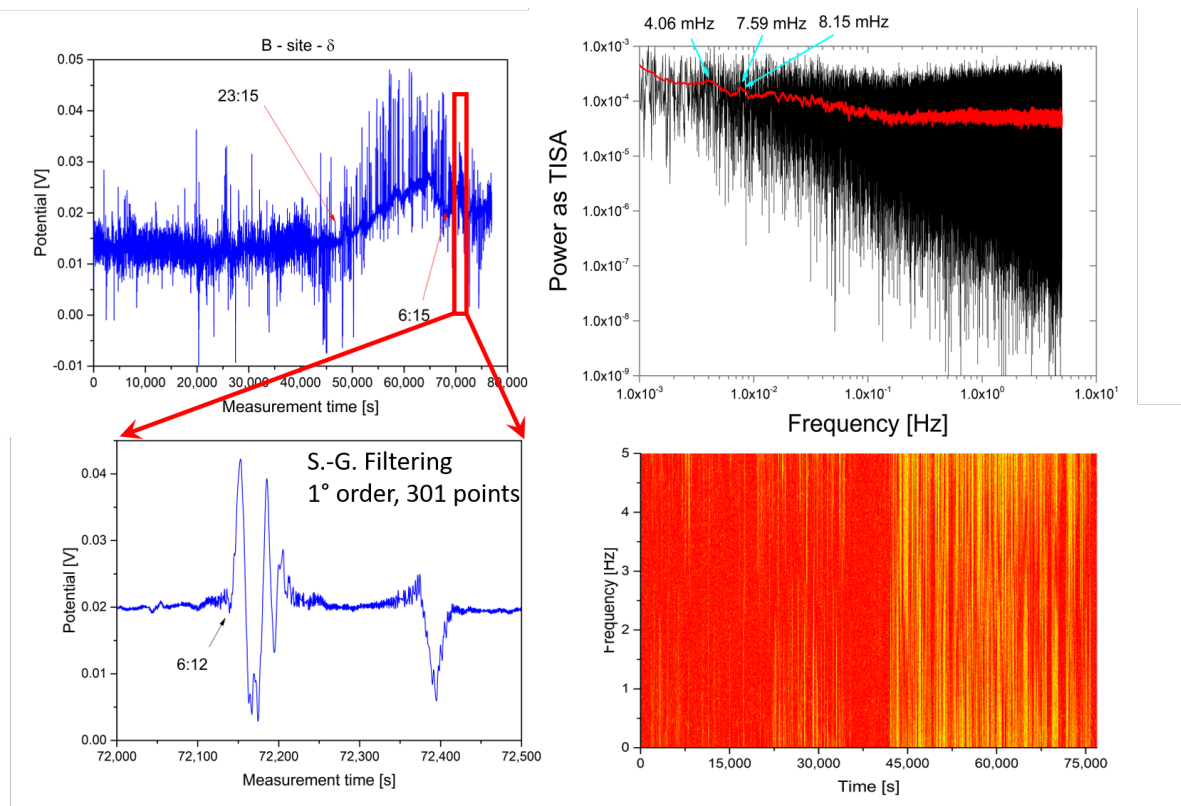


Figure 3. Data measured from site B, tree B2, over ten individual electrodes. Two magnification steps are shown, including the Fast Fourier Transform analysis as Total Impulse Square Amplitude and the Short Time Fourier Transform map.

The effects of sun and moon movement can also be sensed, in particular, Figure 4 reports the stacked curves and some magnified portions of one single channel, to evidence the differences in noise and spike patterns of the signal. Unfortunately sunset/moon rise and sunrise/moon set are too close to clearly resolve in time their effects on the electrical response. The propagation speed of the pseudo peaks along the channels has been calculated to be 0.125 ± 0.005 m/s.

Channels show the following features (see Figure 5): number of spikes, barcode entropy, Simpson index, Space filling, Kolmogorov entropy have the same features, while Signal entropy and Expressiveness have a structure that resembles the modulus of the first derivative of the previous quantities (a peak can be observed where an increasing/decreasing slope is present); Tsallis and Rényi entropies appear to be poorly or not correlated to the previous entities. The number of spike-like peaks detected by the numerical algorithm is higher for channels closer to the leaves and minimal close to the roots; it shows the following structure: a basal line of number of spikes that has a maximum around midday, and a huge peak on top of the baseline with the maximum at midnight. This is less evident for channels close to the roots.

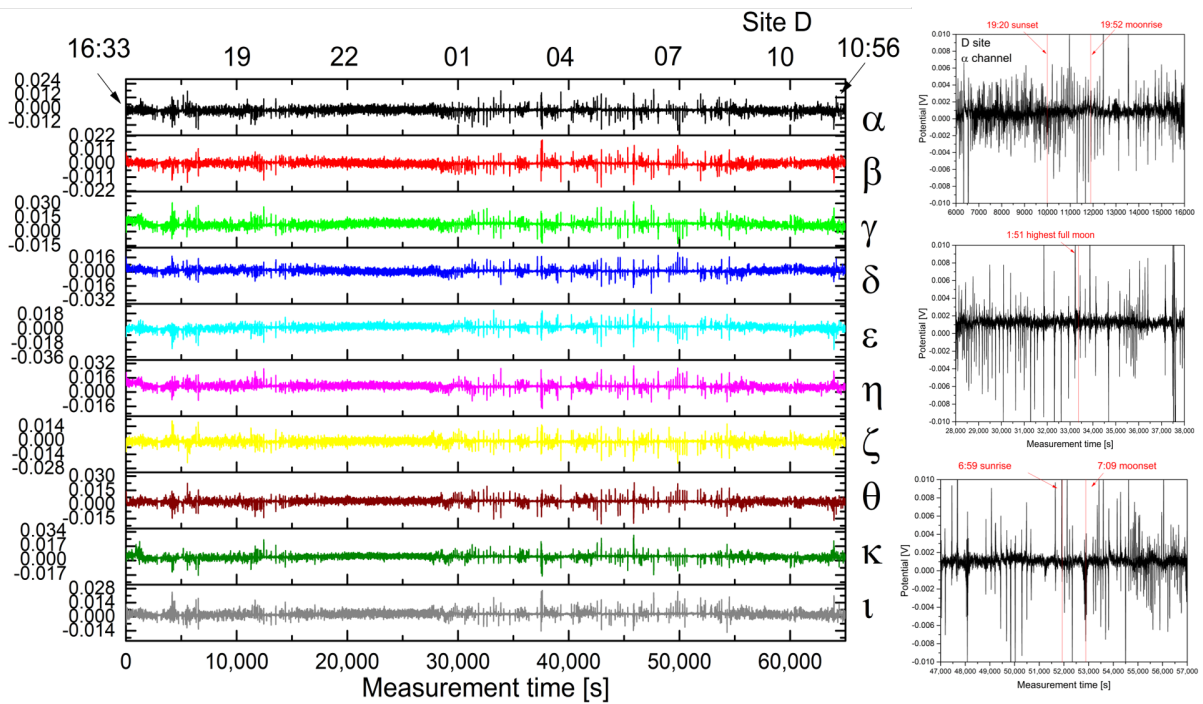


Figure 4. Data measured from site D, tree D1, over ten individual electrodes during the autumn equinox, with full moon and clear sky.

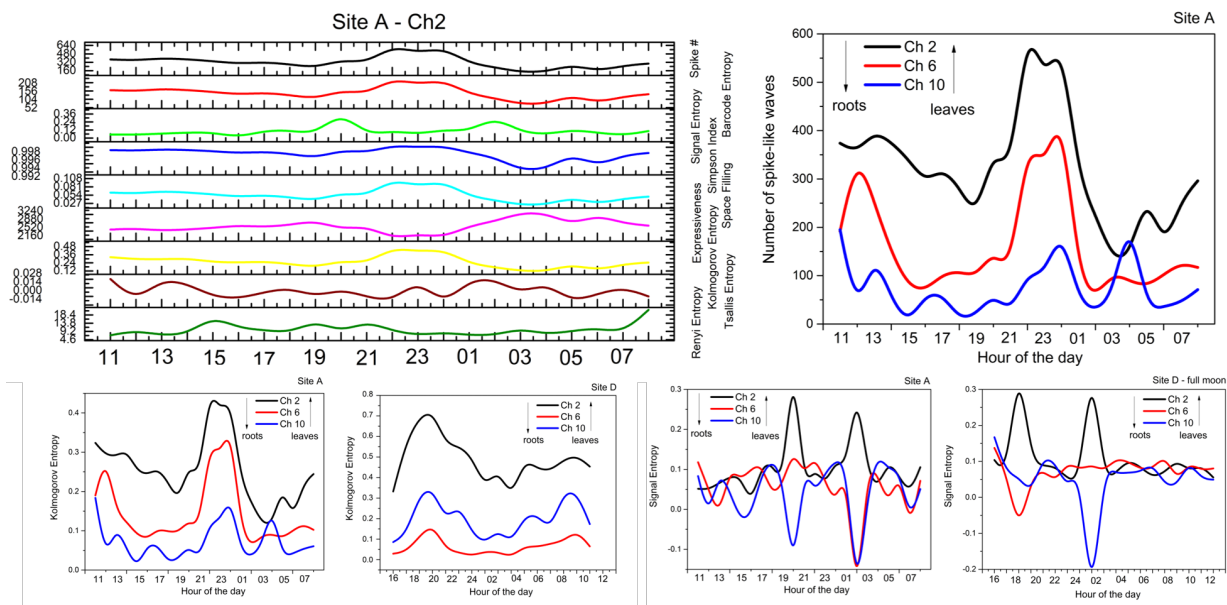


Figure 5. **Top left:** number of spikes, barcode entropy, Simpson index, space filling, Kolmogorov entropy, signal entropy, expressiveness, Tsallis entropy, and Renyi entropy for a selected channel of a selected tree of a selected site. **Top right:** number of spikes for a selected channel of a selected tree of a selected site. **Bottom,** from left to right: Kolmogorov entropy of two selected channels of a selected tree of a selected site, Signal entropy of two selected channels of a selected tree of a selected site.

The signal entropy shows a correlation among all channels between the same site, though it is not possible to conclude anything relevant from the curve analysis. Kolmogorov entropy shows a structure similar to the number of spikes, featuring slightly fewer fluctuations and a clean curve that can track well the plant metabolic activity, or the response to atmospheric phenomena. We can see that, normally, the channel closer to the leaves features higher entropies and that a structure with two peaks per day is preserved. Signal

entropy shows very interesting features. Both site A and D have two peaks around 7 p.m. and 2 a.m. Furthermore, site D shows a negative signal entropy for the stub-positioned channels.

Visualizing the histograms reporting peak duration and amplitudes one might discern between an active plant, featuring a higher diversity with both short spikes and longer periods, and a “dead” stub, where the diversity is very much reduced (see Figure 6). The FFT shows slow activity, particularly enhanced at frequencies around 100 mHz and below. A careful analysis of the E site, corresponding to a sector entirely occupied by stubs, shows how some of them are locked and pretty much correlated. The two-dimensional map proposed here shows the Kolmogorov entropy in color scale, against measurement time and recording channel. Similar color patterns against time are found in closer stubs (# and * symbols).

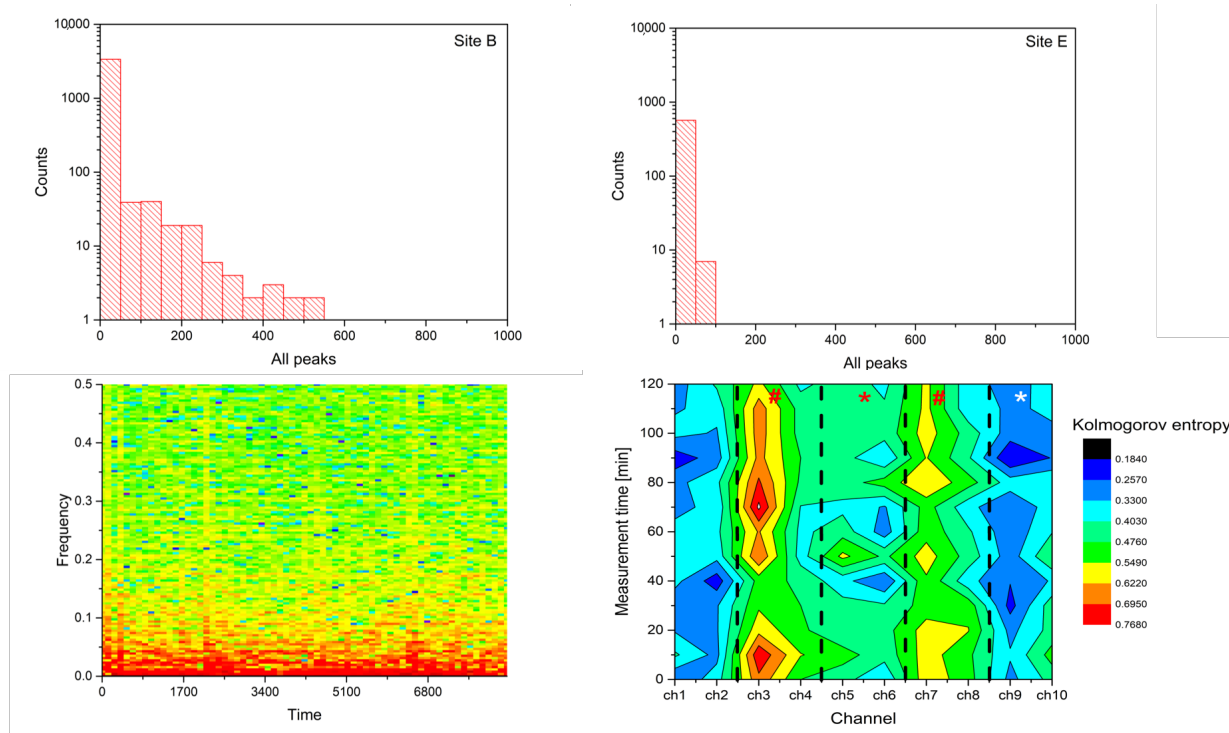


Figure 6. Top row: histograms of the population of spike-like structures detected on different sites. Bottom row, left: FFT map of a selected channel. Right: two-dimensional map of the Kolmogorov entropy over the site populated by stubs. Symbols identify correlated stubs, dashed lines separate the couple of electrodes that work together in differential mode.

Summarizing, we list our results:

1. biopotential features of xylem biomolecular activity can be correlated with the solar (and lunar) cycle (see Figures 3 and 4);
2. statistical features of spike-like peaks and entropy can be derived to visualize time-varying features of underlying molecular processes (see Figure 5).
3. tree stubs show an electrical molecular activity that is correlated with that of neighboring trees (see Figure 6);

In the following, we will see how the Kolmogorov entropy of the bioelectrical signals can be correlated with the Shannon entropy of thermographies, giving a qualitative matching of very distant phenomena, underlying a common hidden basis: the molecular processes. Particularly interesting is to see how the nocturnal temperature of trees is slightly higher than the resting temperature of the environment, which suggests a mechanism to avoid freezing of the wood (appearing as an interesting manifestation of the Le Chatelier principle; see Section 3.1 and Figure 7).

3.1. Theoretical Modelling

3.1.1. Correlation Fields and Dissipative Dynamics

Individual trees exchange energy and matter in different forms with their environment. They are in this sense “open” systems driven by dissipative dynamics under endogenous and external stimuli. We use the word ‘dissipative’ (and ‘dissipation’) in the sense that trees not only release to but also receive from the environment energy and matter.

In their dissipative dynamics, trees go through continuous adjustments of their equilibrium state, undergoing transitions through different dynamical regimes (*phase transitions*) triggered by changes in temperature, pressure, and by other stimuli of external or endogenous origin. In each one of these regimes, the dynamical equilibrium with the environment is obtained according to general physical laws, as it happens in any other biological and physical system.

The general laws of thermodynamics require the minimization of the free energy $\mathcal{F} = U - TS$, namely $d\mathcal{F} = dU - TdS = 0$, at each equilibrium (or quasi-equilibrium) state at a given temperature T , which expresses the first principle of thermodynamics for a system coupled to the environment at constant T and in the absence of mechanical work. For simplicity, we set equal to one the Boltzmann constant k_B . U and S denote the internal energy and the entropy, respectively. Heat is $dQ = TdS$, as usual.

As is well-known, water plays a decisively central role in the tree vital processes and is subject to gradient forces of different origin (gravitation, piezometric pressure, heating and cooling gradients, chemical gradients, friction, etc.). The quantum electronic shells of water molecules present the charge distribution of an electric dipole. There is no preferred direction along which on average the molecular electrical dipoles point. The Lagrangian of the system, expressed in terms of these quantum dipole fields $\psi(\mathbf{x}, t)$, is thus invariant under the transformations of the group of dipole spherical rotations. There is thus symmetry under the SU(2) rotation group. The polarization density $P(\mathbf{x}, t)$ of the system of water molecules is zero.

Referring to the molecular symmetry properties and to the role played by them, as mentioned in the Introduction, the molecular dipole SU(2) rotation symmetry appears thus to be a good symmetry candidate for consideration. It refers to the very specific electric dipole property characterizing all biomolecules and their solvent, i.e., the water molecules in which they are embedded. Although it is quantitatively specific from a molecular standpoint, however, it has the property of being general, able to extend to all of the system molecules.

The electric dipole SU(2) symmetry is, however, *broken* by the mentioned forces acting on the water, which manifests in the polarization density $P(\mathbf{x}, t)$ of non-zero value for some time intervals of the system ground state, which therefore does not have the SU(2) symmetry of the Lagrangian [27–31].

The Breakdown mechanism of the Symmetry (BS) is well known in Quantum Field Theory (QFT). Here we do not consider the explicit BS induced by a change in the system Lagrangian, but the Spontaneous BS (SBS), where the symmetry breaking agent acts, as a trigger on the system states, not changing the Lagrangian [32–35].

According to the Goldstone theorem in QFT, SBS induces the dynamical formation of long-range ordering correlations among the system components, i.e., in the present case, long-range dipole waves among the molecular dipole fields. These dipole waves thus span domains of linear sizes comparable to their propagation (long) range, and are damped or enhanced according to several different, variable boundary conditions.

The quanta associated to the dipole waves are called Nambu-Goldstone (NG) fields, or quanta. In the QFT infinite volume limit, the NG quanta are massless boson modes that condense in coherent way in the system ground state. ‘Coherent’ means that long-range correlations co-exist in the ordered patterns without negative interferences, so that the NG quanta, the Dipole-Wave-Quanta (DWQ) in the present case, behave approximately as an ideal gas of (quasi-)free particles. A measure of the ordering degree of the dipoles

is provided by the non-zero value of a field, in the present case the polarization density $P(\mathbf{x}, t)$, called the ‘order parameter’.

Boundary effects (due to surfaces, impurities, etc.) may result in the non-zero effective mass m_{eff} of the DWQ fields. Dipole wave correlations extend accordingly over coherent domains of finite size of the order of $R = \hbar/(m_{eff}c)$, where c is the speed of light, $\hbar = h/(2\pi)$, and h the Planck constant.

The de Broglie wavelength of the DWQ quantum of momentum p is $\lambda = h/p$. In the DWQ ideal gas approximation, we have $p^2/(2m_{eff}) = (3/2)k_B T$, with k_B the Boltzmann constant. Using $R = n\lambda/2$, with n an integer number, we obtain [31]

$$T = \frac{\pi \hbar c n^2}{6k_B R}. \quad (2)$$

This equation shows that changes in temperature (due to dissipation) influence the range R spanned by dipole wave correlations, and vice versa; thus it sheds some light on the reported experimental observations of thermal spectra in connection with the trees reactivity to environmental stimuli, as commented on below.

Equation (2) suggests that a control mechanism may be at work, aimed at keeping constant the tree temperature, or to limit its variations within an interval convenient for the tree survival (also consistent with the Le Chatelier principle on system reactions opposing external actions perturbing their (thermodynamic) equilibrium [36,37]). Suppose that an external agent produces an increase (decrease) in the temperature. Then the tree dynamic reaction aimed to keep T constant will *oppose* a decrease (increase) of T by increasing (decreasing) the size R of the coherent dipole wave propagation, according to Equation (2). What happens at night, when external temperature drops, is counterfaced by plants’ decreasing R , which is then reflected in a higher frequency of the electrical activity, as indeed observed above (cf. Section 3). It is clear, but worth stressing again, that in the described processes a crucial role is played by dissipativity, namely that the system at molecular scale is an open system, in permanent interaction with the environment.

In Appendix A.1, we show that Equation (2) expresses indeed, at the microscopic dynamical level, the free energy minimization constraint for the equilibrium state, $dU = TdS$. From Equations (A1), (A3) and (A4), we see that variations in T actually imply entropy variations dS , namely ordering/disordering (S decrease/increase) through variations dR of the range over which dipole correlations extend. In these processes, there is energy ‘transmutation’ $U \leftrightarrow TS$, of part of the energy from configurations with higher internal (kinetic) energy content, to more ‘ordered’ ones or, vice versa, part of the energy ‘stored’ in the ordering correlations is ‘disinvested’, i.e., released to obtain higher kinematic freedom (shorter range or loss of correlations, S increases).

We thus see that a remarkable dynamic internal degree of freedom is built in to the system [38]. The single equation $d\mathcal{F} = 0$ for the equilibrium constraint at constant T and V , is of course not enough to uniquely determine the values of the two variables dU and dS . Thus, the system dissipative dynamics, namely its being ‘open’ to external inputs, allows that a transfer (transmutation) of energy is allowed from random kinematics to order and viceversa, as described by ‘moving’ on the straight line of slope $T = dU/dS$ in the plane (U, S) .

The reported experimental measurements of Figure 7 show that the response by the trees to the environment’s large gradients of temperature is such that their temperature does not align with the environment temperature. Instead, a sort of defense reaction or control mechanism is activated thus avoiding the tree’s excessive cooling down, possibly dangerous to their survival. According to the needs (dissipation), energy is stored in the ordering coherent dipole wave correlations, or taken from them. The entropic fingerprint of thermographies, if compared to that of the electrical signals recorded (see Figure 7), shows quantitatively the same features, highlighting the metabolic and connection activity of trees. In particular, we can see how along the time scale (between 2 p.m. and 12 a.m.) we can find two hours of maximum entropy, approximately around 5 p.m. and 9 p.m., where both

the bioelectrical signal and the thermographies experience a higher complexity. In fact, underlying molecular phenomena, although hidden from the measurement standpoint, emerge with their fingerprint.

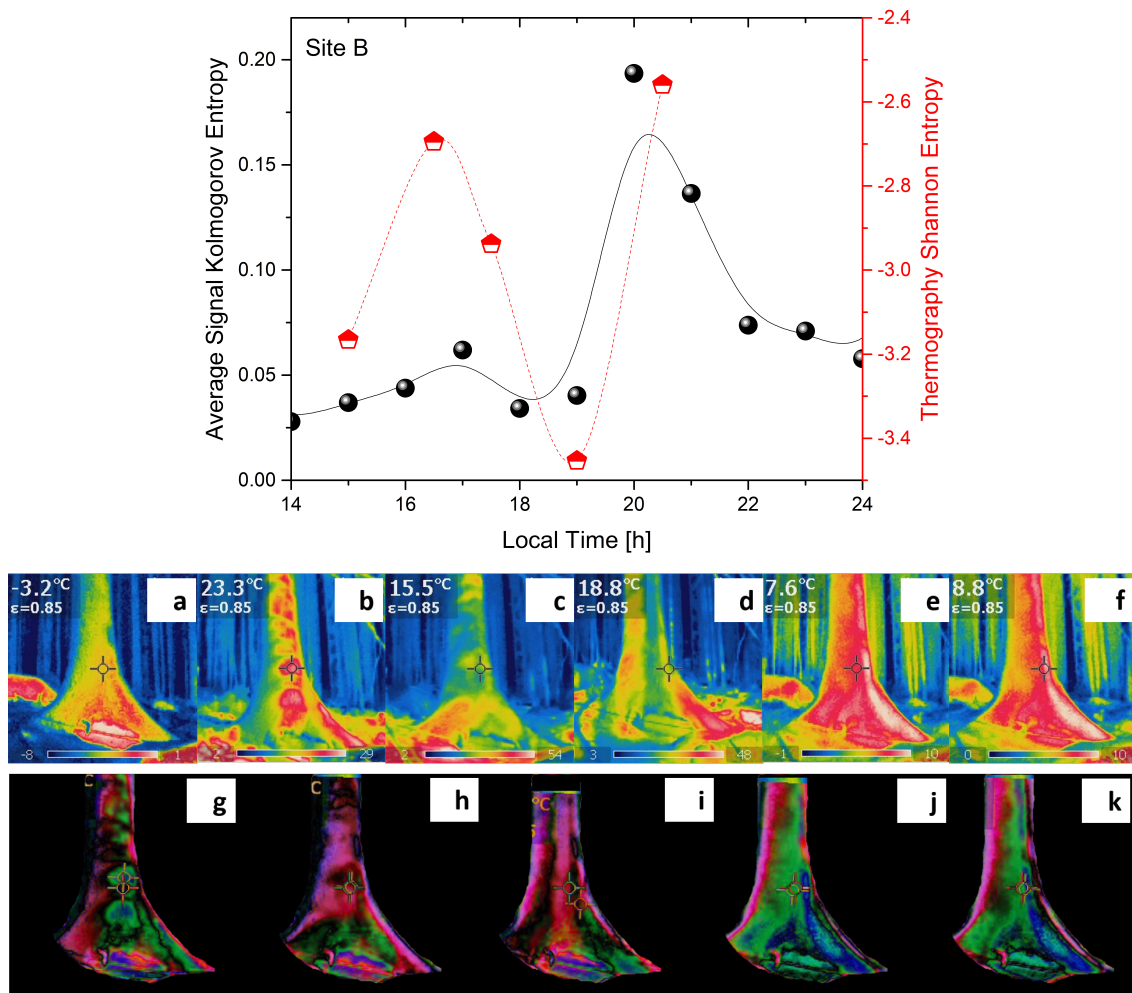


Figure 7. Top: qualitative matching between Kolmogorov entropy computed from the biopotential signal, averaged over the electrodes of site B, and Shannon entropy computed from the thermographies shown in the right panel, shot from the same site B. **Bottom:** thermographies of a *Picea abies* trunk approximately 100 years old in site B (panels a–f) and algebraic difference between the registered frames above, which better allows noticing changes in temperature distribution (panels g–k).

3.1.2. Electromagnetic Field and Collective Dynamical Effects

To study the connection between DWQ of long-range molecular correlations with the reported measures of the electromagnetic (em) field, we limit our discussion to the space components of the em vector potential $\mathbf{A}(\mathbf{x}, t)$ of $A_\mu(\mathbf{x}, t)$ and use the Coulomb gauge condition $\nabla \cdot \mathbf{A}(\mathbf{x}, t) = 0$. When the em field is considered in the Lagrangian, this is invariant under local (and global) U(1) gauge transformations

$$\mathbf{A}(\mathbf{x}, t) \rightarrow \mathbf{A}(\mathbf{x}, t) + \nabla\lambda(\mathbf{x}, t), \quad (3)$$

with $\nabla^2\lambda(\mathbf{x}, t) = 0$ imposed by the condition $\nabla \cdot \mathbf{A}(\mathbf{x}, t) = 0$. The global U(1) symmetry of the ground state is the one surviving the SBS of the spherical SU(2) symmetry of the dipole field $\psi(\mathbf{x}, t)$. However, this global U(1) symmetry is also spontaneously broken since it would be not possible to change simultaneously at every space-point by a constant amount λ the phase of the dipole field $\psi(\mathbf{x}, t)$ in the ground state. SBS of the global U(1) is expressed by the non-zero value of the order parameter $v(\mathbf{x}, t)$, related to $P(\mathbf{x}, t)$ as $|v(\mathbf{x}, t)|^2 = 2P(\mathbf{x}, t)$ [31,35].

The wave function $\sigma(\mathbf{x}, t)$ of the charge density $\rho(\mathbf{x}, t)$, is

$$\sigma(\mathbf{x}, t) = \sqrt{\rho(\mathbf{x}, t)} e^{i\chi(\mathbf{x}, t)}, \quad (4)$$

where the phase is the real field $\chi(\mathbf{x}, t)$, and is related to $v(\mathbf{x}, t)$: $|\sigma(\mathbf{x}, t)|^2 = \rho(\mathbf{x}, t) \propto |v(\mathbf{x}, t)|^2$. The phase $\chi(\mathbf{x}, t)$ represents the NG wave field associated to the U(1) SBS [29,31,34]. The coherent condensation of the $\chi(\mathbf{x}, t)$ quanta in the ground state is induced by the transformation

$$\chi(\mathbf{x}, t) \rightarrow \chi(\mathbf{x}, t) + \frac{q}{\hbar c} \lambda(\mathbf{x}, t), \quad (5)$$

generating the (phase) transformation: $\sigma(\mathbf{x}, t) \rightarrow \exp[i(q/\hbar c) \lambda(\mathbf{x}, t)] \sigma(\mathbf{x}, t)$.

The local gauge invariance of the Lagrangian allows the transformation $\mathbf{A}(\mathbf{x}, t) \rightarrow \mathbf{A}'(\mathbf{x}, t) = \mathbf{A}(\mathbf{x}, t) + (\hbar c/q) \nabla \chi(\mathbf{x}, t)$, and then the transformation $\mathbf{A}'(\mathbf{x}, t) \rightarrow \mathbf{A}'(\mathbf{x}, t) + \nabla \lambda(\mathbf{x}, t)$ is induced by the $\chi(\mathbf{x}, t)$ boson condensation (5), with the constraint $\nabla^2 \chi(\mathbf{x}, t) = 0$ (and $\nabla^2 \lambda(\mathbf{x}, t) = 0$) due to the gauge condition $\nabla \cdot \mathbf{A}(\mathbf{x}, t) = 0$ ($\nabla \cdot \mathbf{A}'(\mathbf{x}, t) = 0$).

Provided that such a gauge constraint is satisfied, $\lambda(\mathbf{x}, t)$ can be a constant or a space–time dependent function, producing homogeneous or non-homogeneous condensate structures in the system ground state, respectively.

For topologically non-trivial $\lambda(\mathbf{x}, t)$, boson condensation may describe vortices, rings, and other extended objects with topological singularities [29,33,35,39]. Since singularities are not compatible with non-zero mass m_{eff} of NG quanta, appearing due to boundary effects [33,35,39], topologically non-trivial extended objects cannot form near the system boundaries. For singular λ , non-commutativity of derivatives, e.g., $(\partial_1 \partial_2 - \partial_2 \partial_1) \lambda(\mathbf{x}, t) \equiv [\partial_1, \partial_2] \lambda(\mathbf{x}, t) \neq 0$, denotes the non-equivalence between different paths connecting two points A and B and the em field $F_{\mu\nu}$ is not invariant under the gauge transformation. Then, observable effects appear [29,39]. On the contrary, no observable effects are produced by regular (non-divergent or topologically trivial) gauge functions.

The above remarks are not of pure mathematical interest; they show in fact the direct connection of the microscopic molecular dynamics with “classical” observations of the behavior of electric and magnetic field. The long-distance electrodynamic intermolecular forces, whose experimental evidence has been recently reported [40], find their microscopic origin at the quantum level in such a theoretically predicted [29,39] connection of the underlying quantum dynamics with the classical electromagnetic fields. The *classical* vector potential evolution equation is indeed directly conditioned by the transformation $\mathbf{A}(\mathbf{x}, t) \rightarrow \mathbf{A}(\mathbf{x}, t) + (\hbar c/q) \nabla \chi(\mathbf{x}, t)$, with topologically non-trivial boson condensation function $\chi(\mathbf{x}, t)$ [29,34,35,39].

In the dissipative dynamics, mathematical consistency requires [33–35,41] that the state of the system of DWQ at temperature T is given by the two modes SU(1,1) generalized coherent state [42]

$$|0(\theta(\beta))\rangle = \prod_{\mathbf{k}} \frac{1}{\cosh \theta_{\mathbf{k}}(\beta)} \exp \left(\tanh \theta_{\mathbf{k}}(\beta) a_{\mathbf{k}}^{\dagger} \tilde{a}_{\mathbf{k}}^{\dagger} \right) |0\rangle, \quad (6)$$

with $\beta = 1/k_B T$, whose time dependence, $\beta = \beta(t)$, is not explicitly shown for notational simplicity. $|0(\theta(\beta))\rangle$ is normalized to 1, $\langle 0(\theta(\beta)) | 0(\theta(\beta)) \rangle = 1$, $\forall \theta(\beta)$, $\forall \beta$, $\forall t$. The operators $a_{\mathbf{k}}^{\dagger}$ and $a_{\mathbf{k}}$ are the NG DWQ creation and annihilation operators, respectively, in terms of which the NG correlation field $\chi(\mathbf{x}, t)$ is expanded. The operators $\tilde{a}_{\mathbf{k}}^{\dagger}$ and $\tilde{a}_{\mathbf{k}}$ are the creation and annihilation operators representing the tree’s environment (the reservoir or thermal bath). In QFT, finite temperature states are indeed condensates of the couples $(a_{\mathbf{k}}, \tilde{a}_{\mathbf{k}})$, the “double” set of operators, those representing the system $a_{\mathbf{k}}$, and their “images” $\tilde{a}_{\mathbf{k}}$, the “doubled” ones representing its environment. For formal details, see [33–35,41].

It can be shown that states at different temperatures, $T \neq T'$, are orthogonal states in the infinite volume limit $V \rightarrow \infty$:

$$\langle 0(\theta(\beta')) | 0(\theta(\beta)) \rangle |_{V \rightarrow \infty} \rightarrow 0, \quad \forall \beta \neq \beta', \tag{7}$$

or, in the jargon of QFT, they belong to unitarily inequivalent representations of the canonical commutation relations (CCR), which means that they describe different dynamical regimes. This formally specifies the meaning of ‘different dynamical regimes’ referred to above.

As said, at constant volume V and given T , the equilibrium constraint $dU = TdS$ is described as the straight line of slope T in the (U, T) plane. The representation of the CCR at a given β (given T) describes the states on such a straight line. A change $\beta \rightarrow \beta'$ leads to a different dynamical regime $|0(\theta(\beta))\rangle \rightarrow |0(\theta(\beta'))\rangle$, i.e., a change in the slope of the straight line in the (U, T) plane, a new ratio dU/dS between internal (kinetic) energy and energy stored in the dipole wave ordering correlations.

The entropy S_a and $S_{\bar{a}}$ can be defined for each of the modes $a_{\mathbf{k}}$ and $\bar{a}_{\mathbf{k}}$, respectively. See Appendix A.2 for the details and the derivation of the Bose–Einstein distribution function at the minimization of free energy. At $d\mathcal{F}_a = dU_a - (1/\beta)dS_a = 0$ one also obtains

$$dU_a = \sum_{\mathbf{k}} \hbar \omega_{\mathbf{k}} \dot{\mathcal{N}}_{a_{\mathbf{k}}}(t) dt = \frac{1}{\beta} dS_a = dQ_a. \tag{8}$$

where $\dot{\mathcal{N}}_{a_{\mathbf{k}}}$ is the time derivative of $\mathcal{N}_{a_{\mathbf{k}}}(\theta(\beta(t)))$, the number of $a_{\mathbf{k}}$ modes condensed in $|0(\theta(\beta))\rangle$. Equation (8) explicitly shows that time variations of the number of $a_{\mathbf{k}}$ modes condensed in the ground state $|0(\theta(\beta))\rangle$ manifest as heat dQ_a (and vice versa). These variations of $\mathcal{N}_{a_{\mathbf{k}}}$ are actually variations in the dipole wave ordering correlations and produce changes by the same quantity (in sign and amount) dQ_a in internal energy dU_a and in entropy dS_a . As one moves out of the $d\mathcal{F}_a = 0$ condition, with $\theta_{\mathbf{k}} \rightarrow \theta'_{\mathbf{k}}$, for small $\delta\theta_{\mathbf{k}} = \theta'_{\mathbf{k}} - \theta_{\mathbf{k}}$ and negligible $\partial\delta\theta_{\mathbf{k}}/\partial t$, the rate of change $\dot{\mathcal{N}}_{a_{\mathbf{k}}}$ induces the change in the entropy

$$\Delta \sum_{\mathbf{k}} \hbar \omega_{\mathbf{k}} \dot{\mathcal{N}}_{a_{\mathbf{k}}}(t) dt = \sum_{\mathbf{k}} 2\dot{\theta}_{\mathbf{k}}(t) \cosh(2\theta_{\mathbf{k}}(t)) \delta\theta_{\mathbf{k}} dt = \frac{1}{\beta} (dS'_a - dS_a), \tag{9}$$

related with the Kolmogorov entropy in nonlinear dynamical systems [43]. In Equation (9), $\dot{\theta}_{\mathbf{k}}(t) \equiv \partial\theta_{\mathbf{k}}(t)/\partial t$.

Since $S_a - S_{\bar{a}}$ is a constant of motion, $dS_a = dS_{\bar{a}}$, i.e., $dQ_a = dQ_{\bar{a}}$, explicitly showing the (dissipative) coupling with the environment. The state $|0(\theta(\beta))\rangle$ is in fact an entangled state for the $a_{\mathbf{k}}$ and $\bar{a}_{\mathbf{k}}$ modes. A quantitative measure of the entanglement is given by the linear correlation coefficient $J(N_a, N_{\bar{a}})$ [44,45] (for simplicity we omit the subscript \mathbf{k}):

$$J(N_a, N_{\bar{a}}) = \frac{cov(N_a, N_{\bar{a}})}{(\langle(\Delta N_a)^2\rangle)^{1/2} (\langle(\Delta N_{\bar{a}})^2\rangle)^{1/2}}, \tag{10}$$

defined for non-zero values of $\langle(\Delta N_a)^2\rangle$ and $\langle(\Delta N_{\bar{a}})^2\rangle$, with $\langle(\Delta N)^2\rangle \equiv \langle(N - \langle N \rangle)^2\rangle = \langle N^2 \rangle - \langle N \rangle^2$ for the variance; the covariance is given by $cov(N_a, N_{\bar{a}}) \equiv \langle N_a N_{\bar{a}} \rangle - \langle N_a \rangle \langle N_{\bar{a}} \rangle$. The symbol $\langle ** \rangle$ denotes expectation value in $|0(\theta(\beta))\rangle$. For non-correlated modes it is $\langle N_a N_{\bar{a}} \rangle = \langle N_a \rangle \langle N_{\bar{a}} \rangle$ and the covariance is zero. For $|0(\theta(\beta))\rangle$ it is $J(N_a, N_{\bar{a}}) = 1$. Recalling that $a_{\mathbf{k}}$ and $\bar{a}_{\mathbf{k}}$ are modes of the DWQ field $\chi(\mathbf{x}, t)$, which is a ‘‘phase’’ field (it appears in the phase, cf. Equation (4)), we showed that entanglement describes phase correlations. These manifest their effects also at a macroscopic level due to the coherent structure of the state $|0(\theta(\beta))\rangle$. In fact, as already mentioned, the boson condensation structure controls the electromagnetic equation at a classical level [29,34,35,39].

The emerging picture is the one of the tree entangled, through its molecular dynamics, with its environment, ‘in-phase’ with it. In the case other trees are in the environment, the

entanglement “among trees” sheds new light on the ‘notion’ of *forest*, in some sense its ‘definition’, *the forest as an in-phase collective dynamical system*.

4. Conclusions and Future Prospects

We showed the first outdoor installation measurements of patterns of electrical activity in a *Picea abies* forest, giving proofs of the following: the physiological activity of plants triggered by photosynthesis can be tracked, stubs still kept alive by the nearby living plants can provide electrical signals correlated to their activity. Side characterizations also show the moon’s effect on the bio-electric potentials, and the electronic transport features of plant resin.

While many novel technologies are being developed to improve our daily lives, we suggest, in this experiment, implementing a technology that goes in the direction of understanding the language of trees, eventually of fungi, which have created a universal living network perhaps using a common language (see Figure 8). Messages conveyed along this network could tell us a lot about the health of the forest, eventually also warn us about forthcoming disasters or ecological threats. By going in this radically new direction, we will ultimately explore the feasibility of a living reservoir computing system, with near zero energy requirements.

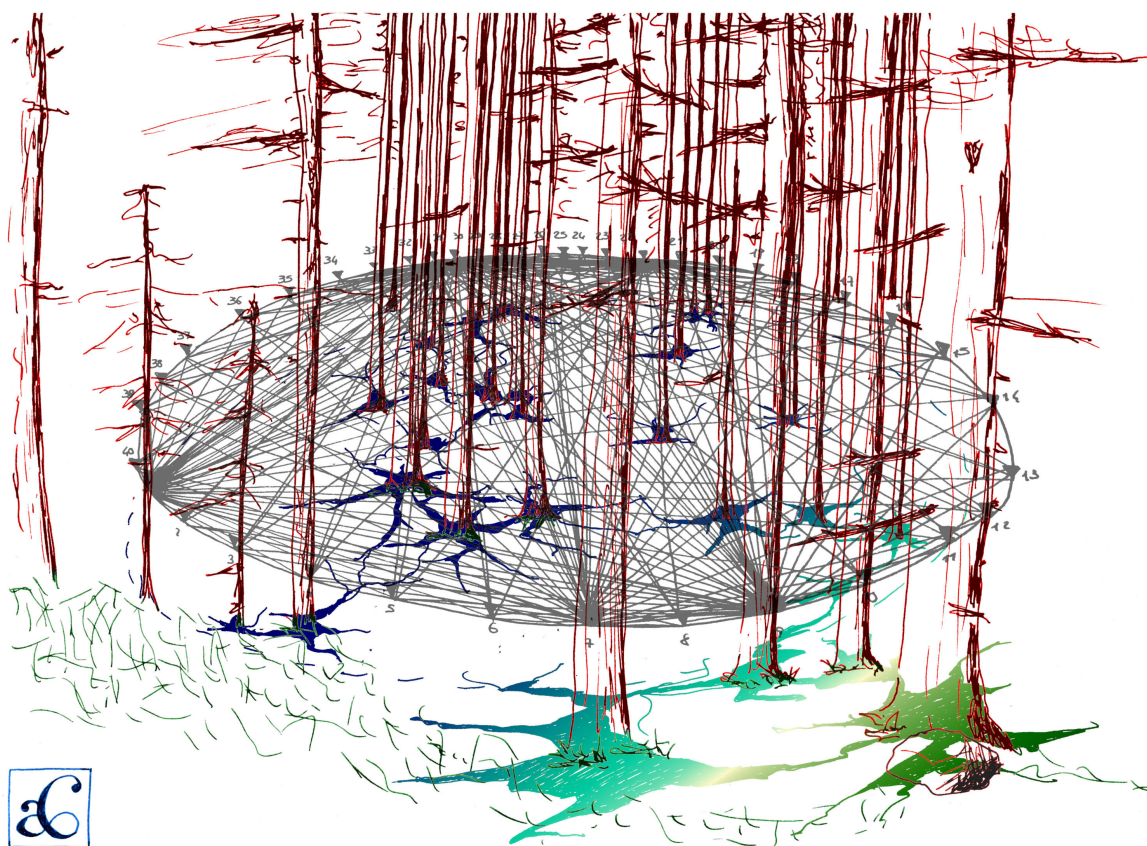


Figure 8. Artist view of the future measurements on the underground Wood Wide Web to map the network geometry by means of electrical tomography.

Author Contributions: Conceptualization, A.C. and A.A.; methodology, A.C.; software, M.M.D.; validation, all; formal analysis, G.V.; data curation, all; writing—original draft preparation, A.C.; writing—review and editing, all; visualization, all; supervision, A.C. All authors have read and agreed to the published version of the manuscript.

Funding: Funding of the activities has been granted by Zenit Arti Audiovisive, Torino, Italy.

Institutional Review Board Statement: Not applicable.

Informed Consent Statement: Not applicable.

Data Availability Statement: Data will be made available by reasonable request to the corresponding authors logging at <https://www.cyberforest.it/> (accessed on 1 January 2020). Data will be made available by reasonable request to the corresponding authors.

Acknowledgments: The authors gratefully acknowledge for the permissions and authorizations to perform the experiments and measurements the Ente Parco Naturale di Paneveggio Pale di San Martino, Provincia Autonoma di Trento, in particular the Administrative Director Fiorella Zortea, and the entire Corpo Forestale at Stazione Forestale Demaniale di Paneveggio e Cadino, in particular Girolamo Scarian. Grateful acknowledgments for their valuable and fundamental contribution to the realization of the entire infrastructure to Alessandro Bernard, Paolo Ceretto and Massimo Arvat. Sincere acknowledgments to the entire workers squad, in particular Piero Baldessari, Andrea Daprà, Ente Parco Naturale di Paneveggio Pale di San Martino, Provincia Autonoma di Trento, the *Genius loci* and Salvanél, Magnifica Comunità della Valle di Fiemme, Renzo Motta and Francesca Secchi, Department of Agricultural, Forest and Food Sciences, University of Turin, Italy. A mention to our sponsors: OpenAzienda S.r.l.S., PrimoPrincipio Società Cooperativa, IGA Technology Services.

Conflicts of Interest: The authors declare no conflict of interest.

Appendix A

Appendix A.1. Derivation of the Minimization of Free Energy from Equation (2)

Consider variations of T , for given n , by differentiating both members of Equation (2):

$$dT = -\frac{A_n}{R^2}dR = Td\left(\log\left(\frac{T}{A}\right)\right), \quad (\text{A1})$$

where it has been put $A_n = \pi hc n^2 / (6k_B)$ and Equation (2) has been repeatedly used. Considering that A_n , for given n , is constant, and since

$$dQ = \frac{dU}{dT}dT; \quad dS = \frac{dQ}{T} = \frac{1}{T} \frac{dU}{dT}dT = \frac{dU}{dT}d(\log T), \quad (\text{A2})$$

where partial derivative notation is not used since we are at constant volume V , Equation (A1) is rewritten as

$$dT = Td(\log T) = TdS \left(\frac{dU}{dT}\right)^{-1}, \quad (\text{A3})$$

which is indeed the minimization condition of the free energy at constant V

$$\left(\frac{dU}{dT}\right)dT = dU = TdS. \quad (\text{A4})$$

Note that the specific heat at constant V of our ‘ideal gas’ of dipole correlation quanta is of course $C_V = dQ/dT = dU/dT$.

Appendix A.2. Entropy, Free Energy and the Bose/Einstein Distribution Function

Entropy S_a and $S_{\tilde{a}}$ can be defined for each of the modes $a_{\mathbf{k}}$ and $\tilde{a}_{\mathbf{k}}$, respectively, they have the same expression, with $\tilde{a}_{\mathbf{k}}$ substituting $a_{\mathbf{k}}$, and $S_a - S_{\tilde{a}}$ is a conserved quantity. One finds:

$$\langle 0(\theta(\beta)) | S_a | 0(\theta(\beta)) \rangle = \sum_{n=0}^{+\infty} W_n \log W_n, \quad (\text{A5})$$

and similarly for $S_{\tilde{a}}$, with

$$W_n = \prod_{\mathbf{k}} \frac{\sinh^{2n_{\mathbf{k}}} \sigma_{\mathbf{k}}}{\cosh^{2(n_{\mathbf{k}}+1)} \theta_{\mathbf{k}}}. \quad (\text{A6})$$

where n stays for the set $\{n_{\mathbf{k}}\}$, $0 < W_n < 1$ and $\sum_{n=0}^{+\infty} W_n = 1$. One also finds

$$|0(\theta(\beta))\rangle = \exp\left(-\frac{1}{2}S_a\right)|\mathcal{I}\rangle = \exp\left(-\frac{1}{2}S_{\tilde{a}}\right)|\mathcal{I}\rangle, \quad (\text{A7})$$

where $|\mathcal{I}\rangle \equiv \exp(\sum_{\mathbf{k}} a_{\mathbf{k}}^\dagger \tilde{a}_{\mathbf{k}}^\dagger)|0\rangle$, and

$$\frac{\partial}{\partial t}|0(\theta(\beta))\rangle = -\left(\frac{1}{2}\frac{\partial S_a}{\partial t}\right)|0(\theta(\beta))\rangle, \quad (\text{A8})$$

with $\beta = \beta(t)$, and similar expression holds with $S_{\tilde{a}}$. Irreversibility of time evolution (*the arrow of time*) thus naturally emerges in the formalism. Equation (A8) shows indeed that entropy controls time evolution, consistently with the dissipative character of the dynamics. The free energy for the a modes is

$$\mathcal{F}_a \equiv \langle 0(\theta(\beta)) | \left(H_a - \frac{1}{\beta} S_a \right) | 0(\theta(\beta)) \rangle, \quad (\text{A9})$$

where $H_a = \sum_{\mathbf{k}} \hbar\omega_{\mathbf{k}} a_{\mathbf{k}}^\dagger a_{\mathbf{k}}$, and similarly for \tilde{a} modes. In the (quasi-)stationary case, the minimization condition $\partial\mathcal{F}_a/\partial\theta_{\mathbf{k}} = 0, \forall \mathbf{k}$, leads to the Bose–Einstein distribution for $a_{\mathbf{k}}$ at time t in $|0(\theta(\beta))\rangle$:

$$\mathcal{N}_{a_{\mathbf{k}}}(t) = \sinh^2 \theta_{\mathbf{k}}(\beta(t)) = \frac{1}{e^{\beta(t)\hbar\omega_{\mathbf{k}}} - 1}, \quad (\text{A10})$$

with $\mathcal{N}_{a_{\mathbf{k}}}(t) = \mathcal{N}_{a_{\mathbf{k}}}(\theta(\beta(t)))$ the number of $a_{\mathbf{k}}$ modes condensed in $|0(\theta(\beta))\rangle$.

Appendix B

Appendix B.1. Resin Electrical Characterization

Resin samples from three conifer species (*Picea abies*, *Cedrus deodara*, and *Larix decidua*) have been characterized for their electronic transport properties, to assess if and how the production of such material by effect of the tree, in the bore hole and consequently in direct contact with the stainless steel electrodes, would influence the measurements. All the resins are highly aromatic and feature a complex composition: the *Picea abies* one is opaque, sticky and semi-solid, the *Cedrus deodara* one is clear, crystalline and fragile, and the *Larix decidua* one is cloudy and fluid as honey. Their composition has been studied in refs. [46,47]. The impedance spectrum shows a broad range of behaviors (see Figure A1), from capacitive to inductive to neutral. In particular it has been found that the *Cedrus deodara*, in the investigated range of frequencies, behaves as an inductor, having a negative reactance that goes to zero at higher frequencies, while the *Picea abies* resin has a capacitive behavior, having a positive reactance that goes to zero with increasing frequencies. The *Larix decidua* resin has a slightly capacitive behavior, featuring a reactance that is hundred-folds smaller than that of the other species. Looking at the resistive component of impedance, we see that *Picea abies* and *Cedrus deodara* show similar values, while the *Larix decidua* sample is three to four orders of magnitude more conductive, probably owing to its liquid nature. Coming to the DC characterization, in the low voltage range applicable to the physiological potentials expressed by the trees, the resin is highly impeditive and shows a similar behavior for all of the species, with some dispersion in the parameters extrapolated from linear fits to the experimental measurements: in particular for *Picea abies* the quality of the fit is reasonable ($R^2 = 0.8$) and the slope (directly proportional to conductivity) is intermediate between the other two species. The high voltage behavior also shows some interesting phenomenology, for what concerns *Picea abies* resin, where we can see a slight memristive behavior, with a symmetrical, pinched hysteresis loop around 60 V of applied potential.

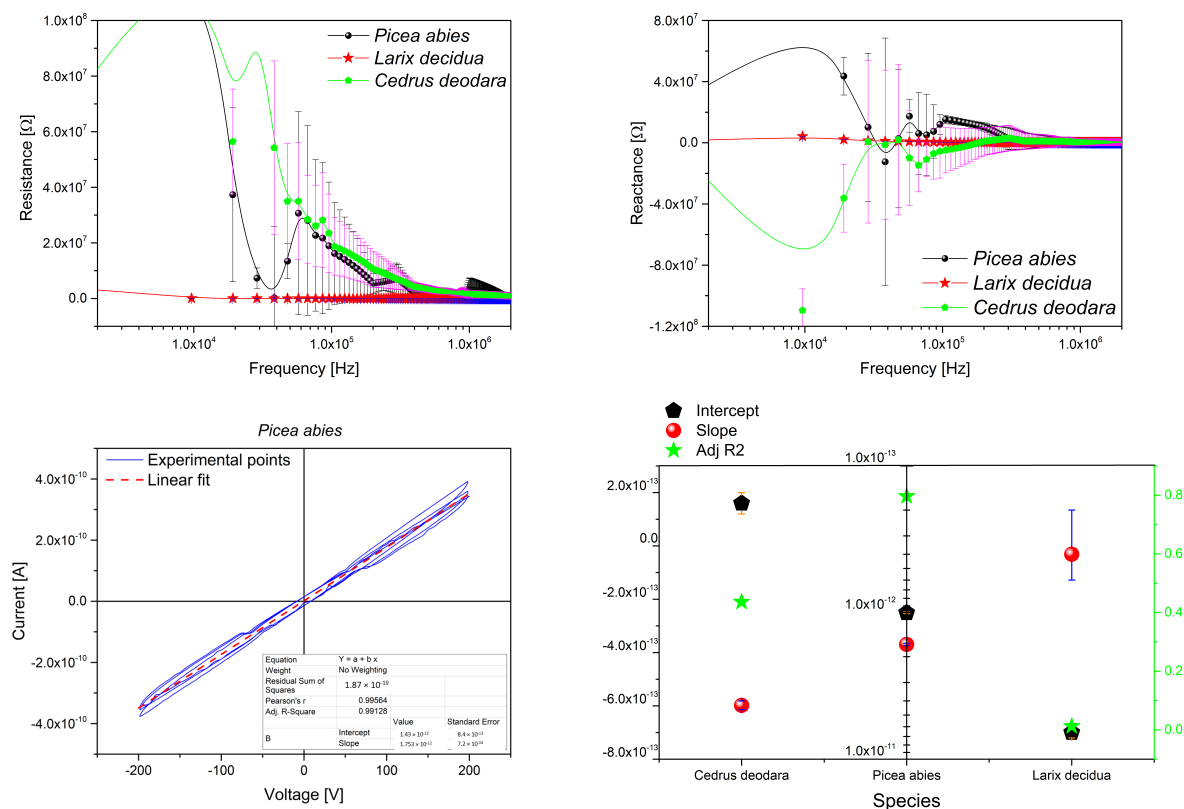


Figure A1. Electronic characterization of several resins: *Picea abies*, *Cedrus deodara*, and *Larix decidua*. **Top row:** impedance measurements, showing resistive (left) and reactive (right) components. **Bottom row:** high voltage range behavior of the *Picea abies* resin (left), and extrapolated linear fit parameters in a comparison between all the three resins (right).

References

1. Tallent-Halsell, N.G. *Forest Health Monitoring: Field Methods Guide*; Technical Report; Environmental Protection Agency: Las Vegas, NV, USA, 1994.
2. Lausch, A.; Borg, E.; Bumberger, J.; Dietrich, P.; Heurich, M.; Huth, A.; Jung, A.; Klenke, R.; Knapp, S.; Mollenhauer, H.; et al. Understanding forest health with remote sensing, part III: Requirements for a scalable multi-source forest health monitoring network based on data science approaches. *Remote Sens.* **2018**, *10*, 1120. [[CrossRef](#)]
3. Alexander, S.A.; Palmer, C.J. Forest health monitoring in the United States: First four years. *Environ. Monit. Assess.* **1999**, *55*, 267–277.
4. Steinman, J. Tracking the health of trees over time on forest health monitoring plots. In *Integrated Tools for Natural Resources Inventories in the 21st Century: An International Conference on the Inventory and Monitoring of Forested Ecosystems, 16–19 August 1998*; Boise, ID. Gen. Tech. Rep. NCRS-212; Mark, H., Thomas, B., Eds.; US Department of Agriculture, Forest Service, North Central Research Station: St. Paul, MN, USA, 2000; pp. 334–339.
5. Coulston, J.W.; Ambrose, M.J.; Riitters, K.H.; Conkling, B.L. *Forest Health Monitoring: 2002 National Technical Report*; Gen. Tech. Rep. SRS-84; US Department of Agriculture, Forest Service, Southern Research Station: Asheville, NC, USA, 2005; Volume 84, 97p.
6. Carrière, S.; Ruffault, J.; Pimont, F.; Doussan, C.; Simioni, G.; Chalikakis, K.; Limousin, J.M.; Scotti, I.; Courdier, F.; Cakpo, C.B.; et al. Impact of local soil and subsoil conditions on inter-individual variations in tree responses to drought: Insights from Electrical Resistivity Tomography. *Sci. Total Environ.* **2020**, *698*, 134247. [[CrossRef](#)] [[PubMed](#)]
7. Al Hagrey, S. Electrical resistivity imaging of tree trunks. *Near Surf. Geophys.* **2006**, *4*, 179–187. [[CrossRef](#)]
8. Luo, Z.; Deng, Z.; Singha, K.; Zhang, X.; Liu, N.; Zhou, Y.; He, X.; Guan, H. Temporal and spatial variation in water content within living tree stems determined by electrical resistivity tomography. *Agric. For. Meteorol.* **2020**, *291*, 108058. [[CrossRef](#)]
9. Ganthaler, A.; Sailer, J.; Bär, A.; Losso, A.; Mayr, S. Noninvasive Analysis of Tree Stems by Electrical Resistivity Tomography: Unraveling the Effects of Temperature, Water Status, and Electrode Installation. *Front. Plant Sci.* **2019**, *10*, 1455. [[CrossRef](#)] [[PubMed](#)]
10. Brenner, E.D.; Stahlberg, R.; Mancuso, S.; Vivanco, J.; Baluška, F.; Van Volkenburgh, E. Plant neurobiology: An integrated view of plant signaling. *Trends Plant Sci.* **2006**, *11*, 413–419. [[CrossRef](#)]

11. Baluška, F.; Mancuso, S.; Volkmann, D. *Communication in Plants: Neuronal Aspects of Plant Life*; Springer: Berlin/Heidelberg, Germany, 2006.
12. Mancuso, S.; Viola, A. *Brilliant Green: The Surprising History and Science of Plant Intelligence*; Island Press: Washington, DC, USA, 2015.
13. Grant, R. Do trees talk to each other? *Smithson. Mag.* **2018**, *180968084*, 1–9.
14. Baluška, F.; Mancuso, S. Plant neurobiology: From sensory biology, via plant communication, to social plant behavior. *Cogn. Process.* **2009**, *10*, 3–7. [[CrossRef](#)]
15. Hedrich, R.; Salvador-Recatalà, V.; Dreyer, I. Electrical wiring and long-distance plant communication. *Trends Plant Sci.* **2016**, *21*, 376–387. [[CrossRef](#)]
16. Gorzelak, M.A.; Asay, A.K.; Pickles, B.J.; Simard, S.W. Inter-plant communication through mycorrhizal networks mediates complex adaptive behaviour in plant communities. *AoB Plants* **2015**, *7*, plv050. [[CrossRef](#)]
17. Hanson, A. Spontaneous electrical low-frequency oscillations: A possible role in Hydra and all living systems. *Philos. Trans. R. Soc. B Biol. Sci.* **2021**, *376*, 20190763. [[CrossRef](#)]
18. Volkov, A.G.; Shtessel, Y.B. Underground electrotonic signal transmission between plants. *Commun. Integr. Biol.* **2020**, *13*, 54–58. [[CrossRef](#)]
19. Adamatzky, A. Language of fungi derived from their electrical spiking activity. *R. Soc. Open Sci.* **2022**, *9*, 211926. [[CrossRef](#)]
20. Tattoni, C.; Ciolli, M.; Ferretti, F.; Cantiani, M.G. Monitoring spatial and temporal pattern of Paneveggio forest (northern Italy) from 1859 to 2006. *iForest-Biogeosci. For.* **2010**, *3*, 72. [[CrossRef](#)]
21. Auricchio, L.; Cook, E.; Pacini, G. 'Fatto di Fiemme': Stradivari's violins and the musical trees of the Paneveggio. In *Invaluable Trees: Cultures of Nature*; Voltaire Foundation: Oxford, UK, 2012.
22. Burckle, L.; Grissino-Mayer, H.D. Stradivari, violins, tree rings, and the Maunder Minimum: A hypothesis. *Dendrochronologia* **2003**, *21*, 41–45. [[CrossRef](#)]
23. Cherubini, P. Tree-ring dating of musical instruments. *Science* **2021**, *373*, 1434–1436. [[CrossRef](#)]
24. Kaspar, F.; Schuster, H. Easily calculable measure for the complexity of spatiotemporal patterns. *Phys. Rev. A* **1987**, *36*, 842. [[CrossRef](#)]
25. Rényi, A. On measures of entropy and information. In *Proceedings of the Fourth Berkeley Symposium on Mathematical Statistics and Probability, Volume 1: Contributions to the Theory of Statistics*; University of California Press: Berkeley, CA, USA, 1961; pp. 547–561.
26. Tsallis, C. Possible generalization of Boltzmann-Gibbs statistics. *J. Stat. Phys.* **1988**, *52*, 479–487. [[CrossRef](#)]
27. Matsumoto, H.; Umezawa, H.; Vitiello, G.; Wyly, J. Spontaneous breakdown of a non-Abelian symmetry. *Phys. Rev.* **1974**, *D9*, 2806–2813. [[CrossRef](#)]
28. Shah, M.; Umezawa, H.; Vitiello, G. Relation among spin operators and magnons. *Phys. Rev.* **1974**, *B10*, 4724–4726. [[CrossRef](#)]
29. Matsumoto, H.; Papastamatiou, N.J.; Umezawa, H.; Vitiello, G. Dynamical rearrangement in Anderson-Higgs-Kibble mechanism. *Nucl. Phys. B* **1975**, *97*, 61–89. [[CrossRef](#)]
30. Del Giudice, E.; Doglia, S.; Milani, M.; Vitiello, G. A quantum field theoretical approach to the collective behaviour of biological systems. *Nucl. Phys. B* **1985**, *251*, 375–400. [[CrossRef](#)]
31. Del Giudice, E.; Doglia, S.; Milani, M.; Vitiello, G. Electromagnetic field and spontaneous symmetry breaking in biological matter. *Nucl. Phys. B* **1986**, *275*, 185–199. [[CrossRef](#)]
32. Itzykson, C.; Zuber, J. *Electromagnetic Field and Spontaneous Symmetry Breaking in Biological Matter*; McGraw-Hill: New York, NY, USA, 1980.
33. Umezawa, H.; Matsumoto, H.; Tachiki, M. *Thermo Field Dynamics and Condensed States*; North-Holland: Amsterdam, The Netherlands, 1982.
34. Umezawa, H. *Advanced Field Theory: Micro, Macro, and Thermal Physics*; AIP: New York, NY, USA, 1993.
35. Blasone, M.; Jizba, P.; Vitiello, G. *Quantum Field Theory and Its Macroscopic Manifestations*; Imperial College Press: London, UK, 2011.
36. Fermi, E. *Termodinamica*; Boringhieri: Torino, Italy, 1958.
37. Landau, L.; Lifshitz, E.M. *Statistical Physics*; Pergamon Press: Oxford, UK, 1958.
38. Kurcz, A.; Capolupo, A.; Beige, A.; Del Giudice, E.; Vitiello, G. Energy concentration in composite quantum systems. *Phys. Rev. A* **2010**, *81*, 063821. [[CrossRef](#)]
39. Matsumoto, H.; Papastamatiou, N.J.; Umezawa, H. The boson transformation and the vortex solutions. *Nucl. Phys. B* **1975**, *97*, 90–124. [[CrossRef](#)]
40. Lechelon, M.; Meriguet, Y.; Gori, M.; Ruffenach, S.; Nardecchia, I.; Floriani, E.; Coquillat, D.; Teppe, F.; Mailfert, S.; Marguet, D.; et al. Experimental evidence for long-distance electrodynamic intermolecular forces. *Sci. Adv.* **2022**, *8*, eabl5855. [[CrossRef](#)]
41. Celeghini, E.; Rasetti, M.; Vitiello, G. Quantum Dissipation. *Ann. Phys.* **1992**, *215*, 156–170. [[CrossRef](#)]
42. Perelomov, A. *Generalized Coherent States and Their Applications*; Springer: Berlin/Heidelberg, Germany, 1986.
43. Hilborn, R. *Chaos and Nonlinear Dynamics*; Oxford University Press: Oxford, UK, 1994.
44. Gerry, C.; Knight, P. *Introductory Quantum Optics*; Cambridge University Press: Cambridge, UK, 2005.
45. Sabbadini, S.; Vitiello, G. Entanglement and phase-mediated correlations in quantum field theory. Application to brain-mind states. *Appl. Sci.* **2019**, *9*, 3203. [[CrossRef](#)]

-
46. Lee, R.A. The Stability of Wood Resin Colloids in Paper Manufacture. Ph.D. Thesis, University of Tasmania, Hobart, Australia, 2012.
 47. Douros, A.; Christopoulou, A.; Kikionis, S.; Nikolaou, K.; Skaltsa, H. Volatile Components of Heartwood, Sapwood, and Resin from a Dated *Cedrus brevifolia*. *Nat. Prod. Commun.* **2019**, *14*. [[CrossRef](#)]